

FY19 Laboratory Basic Science Program

M. S. Wei

Laboratory for Laser Energetics, University of Rochester

In FY19, a total of 25 Laboratory Basic Science (LBS) projects were allocated a total of 27.5 shot days for experiments at the Omega Laser Facility, which included five additional projects selected from the FY19 LBS proposals based on their ranking to back fill some of the National Laser Users' Facility allocations. A total of 289 target shots were conducted for the LBS experiments led by scientists from Lawrence Livermore National Laboratory (LLNL), Los Alamos National Laboratory (LANL), LLE, SLAC, and Princeton Plasma Physics Laboratory (PPPL) (see Table I). The FY19 LBS experiments are summarized here.

Table I: LBS experiments conducted at the Omega Laser Facility in FY19.

Principal Investigator	Institution	Title
F. Albert	LLNL	Laser Wakefield Electron Acceleration and Betatron Radiation on OMEGA EP
H. Chen	LLNL	Exploring the Applications of Laser-Produced Relativistic Electron–Positron Pair-Plasma Jets
H. Chen	LLNL	Laboratory Model of Particle Acceleration in Supernova Shocks
K. Flippo	LANL	Characterizing Magnetized Turbulent Plasmas: Toward Generating Laboratory Dynamo
C. J. Forrest	LLE	Evaluation of Neutron-Induced Breakup with Light-Z Nuclei at $E_n = 14.03$ MeV at the Omega Laser Facility
W. Fox	PPPL	Turbulent Transport in Magnetized HED Plasmas
D. E. Fratanduono	LLNL	Investigating Giant Impacts Between Rocky Planets with High-Pressure Melting and Shock Equation-of-State Measurements on Complex Silicates
A. Gleason	SLAC	Viscosity Measurements Using Tracer Particles
S. Glenzer	SLAC	High-Yield Neutron Pulses from Deflagrating Convergence in Hohlräume
X. Gong	LLE	Structure and Melting of High-Pressure Sodium and Potassium
M. Gorman	LLNL	Phase Transformation Kinetics—Strain Rate Tuning of the Peierls Distortion in Ramp-Compressed BCT Sn
B. J. Henderson	LLE	Optical Spectroscopy of High-Pressure Sodium
S. X. Hu	LLE	Uncharted Territory: Testing the Predictions of Density Functional Theory (DFT) in Warm and Extremely Dense Plasmas
L. C. Jarrott	LLNL	Using Line Intensity Enhancements to Characterize NLTE Plasmas
S. Jiang	LLNL	Characterizing Pressure Ionization in Ramp-Compressed Materials with Fluorescence and Absorption Spectroscopy
G. Kagan	LANL	Probing Electron Distribution in Spherical Implosions with Hard X-Ray Spectroscopy

Table I: LBS experiments conducted at the Omega Laser Facility in FY19 (continued).

Principal Investigator	Institution	Title
S. Khan	LLNL	Absolute EOS Measurements of Low-Density Foams Toward Studying the Landau–Darrieus Instability in HED Conditions
A. Krygier	LLNL	The Strength of Fe and Fe-Si 16 wt% at the Conditions in Earth’s Core
E. Marley	LLNL	Radiative Properties of an Open L-Shell, Non-LTE Plasma
M. Millot	LLNL	A Journey to the Center of Uranus and Neptune: Using X-Ray Diffraction to Unravel the Atomic Structure of New Solid and Superionic Ices at Multi-Megabar Pressures
Z. L. Mohamed	LLE	Study of Gamma Ray Products from Reactions Relevant to Big Bang Nucleosynthesis
J. Moody	LLNL	Developing an Ultrahigh Magnetic Field Laboratory for HED Science
H. G. Rinderknecht	LLNL	Structure and Scaling of Strong Collisional Plasma Shocks
R. Saha	LLE	Measurements of Warm Dense Matter Based on Angularly and Spectrally Dispersed X-Ray Scattering
W. Theobald	LLE	X-Ray Phase-Contrast Imaging of Strong Shocks in Foam Targets

During FY19, LLE issued a solicitation for LBS proposals for beam time in FY20. A total of 36 proposals were submitted requesting a total of 57.5 shot days, 274% exceeding the LBS allocation, showing strong interest and high demand of Omega Laser Facility time for basic high-energy-density (HED) experiments from both National Nuclear Security Administration inertial confinement fusion (ICF) labs and Office of Science laboratories. An independent LBS Proposal Review Committee consisting of 12 experts from university, national laboratories, and industry reviewed and ranked the proposals. Based on the Review Committee’s recommendation, 22 proposals, including one led by Lawrence Berkeley National Laboratory, were selected and allocated a total of 21.5 shot days for experiments at the Omega Laser Facility in FY20 as shown in Table II.

Table II: LBS experiments approved for target shots at the Omega Laser Facility in FY20.

Principal Investigator	Institution	Title
F. Albert	LLNL	X-Ray Radiation Driven by Laser Wakefield Acceleration at OMEGA EP
H. Chen	LLNL	Develop a Magnetic Mirror Trap for Laser-Produced Relativistic Electron–Positrons
F. Coppari	LLNL	The Atomic Structure and Melting of New Solid and Superionic Water Ices at Multi-Megabar Pressures: Searching for Ice XIX
T. Döppner	LLNL	Experimental Measurement of Mutual Diffusivity in Warm Dense Matter
K. A. Flippo	LANL	Quantifying the Path to Saturation in a Turbulent Magnetic Dynamo (TMD)
W. Fox	PPPL	Turbulent Transport in Magnetized HED Plasmas
D. E. Fratanduono	LLNL	Investigating Giant Impacts between Rocky Planets with High-Pressure Melting and Shock Equations-of-State Measurements on Complex Silicates
L. Gao	PPPL	Effect of Laser Parameters on Magnetic Field Generation with Laser-Powered Capacitor Coils
A. Gleason	SLAC	Viscosity Measurements Using Tracer Particles
S. Jiang	LLNL	Characterizing Pressure Ionization in High Density with X-Ray Line Emission Spectroscopy
O. M. Mannion	LLE	Measuring the Gamow Energy Shift of Fusion Products in High-Temperature Plasmas
M. Millot	LLNL	Peering Into the Ice Giant Planets Using Shocks on Precompressed Water–Ammonia Mixtures: Superionic Ammonia Hydrates

Table II: LBS experiments approved for target shots at the Omega Laser Facility in FY20 (continued).

Principal Investigator	Institution	Title
Z. L. Mohamed	LLE	Study of Gamma Ray Products from Reactions Relevant to Big Bang Nucleosynthesis
P. M. Nilson	LLE	Terra Incognita: Testing the Predictions of Density Functional Theory (DFT) in Warm and Extremely Dense Plasmas
A. Pak	LLNL	Proton Radiography of Target Normal Sheath Acceleration Fields in the Long-Pulse Regime
H. G. Rinderknecht	LLE	Measuring the Triton Breakup Reaction T(n,2n)D
R. Saha	LLE	Optical and X-Ray Scattering Measurements of Dense Lithium
R. Smith	LLNL	The Effect of Alloying on High-Pressure Phase Transformations: Diffusion Time Scales and Kinetics
C. Stoeckl	LLE	Development of New Experimental Platform LIANS on OMEGA/OMEGA EP for Deuteron and Triton-Induced Nuclear Reactions
G. Swadling	LLNL	An Investigation of Magnetic Fields Generated by Instability Microphysics in Collisionless Plasmas Flow Interactions Using Optical Thomson Scattering
S. Zhao	LBNL	Extreme Deformation and Failure of High Entropy Alloys by Laser Shock-Induced Compression and Tension
A. B. Zylstra	LLNL	Implsions for Studying Solar CNO Reactions

Laser Wakefield Acceleration on OMEGA EP

Principle Investigator: F. Albert, LLNL

Co-investigators: N. Lemos,* J. Williams, and H. Chen (LLNL); and J. L. Shaw, D. Haberberger, and D. H. Froula (LLE)

Graduate student: P. King (LLNL/University of Texas, Austin)

*Postdoc

This series of shots was designed to accelerate electrons in the self-modulated laser wakefield acceleration (SMLWFA) regime, in collaboration with LLE. The Wakefield-EP-19A shot day was coupled with other LLE-led campaigns (PlasmaLensEP and AdvRadEP), with an overall goal to accelerate high-charge, relativistic electrons beyond 100 MeV. This laser wakefield acceleration platform will serve future applications (development and use of novel x-ray sources) on OMEGA EP and the National Ignition Facility's (NIF's) Advanced Radiographic Capability (ARC) laser.

The shot day alternatively used the backlighter and sidelighter beams in their best compression configuration (0.7-ps pulse duration), focused onto the newly commissioned OMEGA EP ten-inch manipulator (TIM)-based gas-jet system. The gas jet provided plasma electron densities in the 3×10^{18} to 1×10^{19} cm⁻³ range. Since laser wakefield acceleration benefits from longer focal lengths, we used apodizers to increase the effective focal length to $f/6$ ($f/10$) on the backlighter (sidelighter) from the original $f/2$ geometry. This resulted in a maximum energy on target of 95 J (24 J). We used 6-mm-long and 10-mm-long nozzles and varied the laser intensity between 3×10^{18} and 6×10^{19} W/cm².

The campaign successfully measured Maxwellian electron beam spectra up to 200 MeV with the electron-proton-positron spectrometer (EPPS) as well as the beam profile, using two image plates with a hole placed in front of the diagnostic, as shown in Fig. 1. Beam profiles with divergences <100 mrad were measured, with a total charge above 100 nC, which is the highest charge recorded in a self-modulated laser wakefield accelerator to date.

Analysis of the campaigns is ongoing, and the results of the shot day, coupled to the LLE-led campaigns, were presented in an invited talk¹ at the annual 2019 APS-DPP meeting.

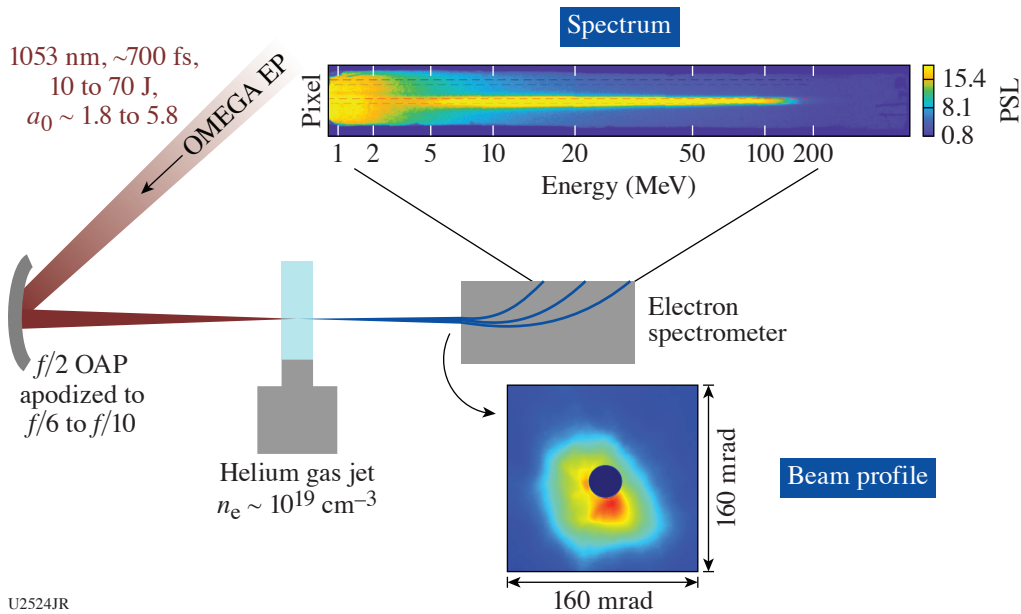


Figure 1
Experimental configuration for Wakefield-EP-19A, with examples of a measured electron spectrum and beam profile.

Exploring the Applications of Laser-Produced Relativistic Electron–Positron Pair-Plasma Jets

Principle Investigator: H. Chen (LLNL)

Co-investigators: J. Kim (UCSD); M. Manuel (GA); and S. Kerr,* A. Macphee, and A. Link (LLNL)

*Postdoc

In FY19, this team completed one LBS shot day on OMEGA EP, alternating the two OMEGA EP short-pulse beams to produce jets of electron–positron antimatter pairs. These 14 FY19 shots used novel targets to explore the laser–target interaction and to seek enhanced pair production. The experiment focused on (1) enhancing the pair yield using nanostructured targets and (2) collimating or focusing positron jets by shaping the rear target surface to modify the sheath potential. The experiments successfully demonstrated both yield enhancement and positron focusing. The data strengthened prospects for future experiments on laboratory astrophysics using the pair jet–plasma interaction to drive beam instabilities.

The OMEGA EP short-pulse beams (~ 1 kJ in 10 ps) irradiated 1-mm-thick Au targets, with and without (1) a parabolic cone on the front of the target and (2) a convex-shaped back surface. It was found that for the same laser energy, positron yields and acceleration were both increased by using the parabolic cones, with a trend similar to that found on NIF ARC experiments.² This finding is important as well as unexpected because the OMEGA EP laser has a smaller f number ($f \sim 2$) compared to that of ARC ($f \sim 60$). The underlying physics remain to be investigated. We also repeated the results obtained in FY18 that used a hemispherical-shaped back surface to focus the positron jets through the sheath field,³ similar to that observed in proton focusing. This observation is important because it demonstrated that higher pair density can be achieved by reducing their volume, which may enable the development of instabilities predicted by theory.

The prior experiments showed that quasi-monoenergetic relativistic positron jets are formed during high-intensity irradiation of thick gold targets,^{4,5} and that these jets can be strongly collimated⁶ using the magneto-inertial fusion electrical delivery system (MIFEDS).⁷ The external field produces a 40-fold increase in the peak positron and electron signals.⁵ The positron yield was found to scale as the square of the laser energy.^{8,9} The FY15 results revealed another dimension of scaling on the target materials.

The favorable scaling would enable the laboratory study of relativistic pair plasmas that are important to understanding some of the most exotic and energetic systems in the universe.^{9,10}

Laboratory Model of Particle Acceleration in Supernova Shocks

Principle Investigator: H. Chen (LLNL)

Co-investigators: C. A. J. Palmer,* A. R. Bell, A. Bott,* G. Gregori, and J. Matthews* (Oxford); D. Lamb and P. Tzeferacos (University of Chicago); A. Birkel and C. K. Li (MIT); and H.-S. Park (LLNL)

Graduate student: O. Karnbach (Oxford)

*Postdoc

This shot day studied the growth of the nonresonant hybrid instability in a turbulent magnetized plasma driven by a high-current proton beam. The TDYNO target platform¹¹ is used to produce a turbulent magnetized plasma. This is generated by colliding the flow of two plasma jets, each of which has had its flow disrupted by passage through a mesh. The jets are produced by ten OMEGA beams with 2 kJ of energy arranged into a 10-ns-long drive. Previous shot days have demonstrated that this can produce plasmas embedded with stochastic magnetic fields with strengths up to 4 kG. One of the OMEGA EP short-pulse beams (2 kJ in 100 ps) was used to produce a proton beam from a thin (50- μm) metal target. This target was positioned 3 mm from the central axis of the turbulent plasma (Fig. 2). The OMEGA EP beam was fired 20 ns after the OMEGA beams so that the low-energy TNSA proton beam would interact with the turbulent plasma.

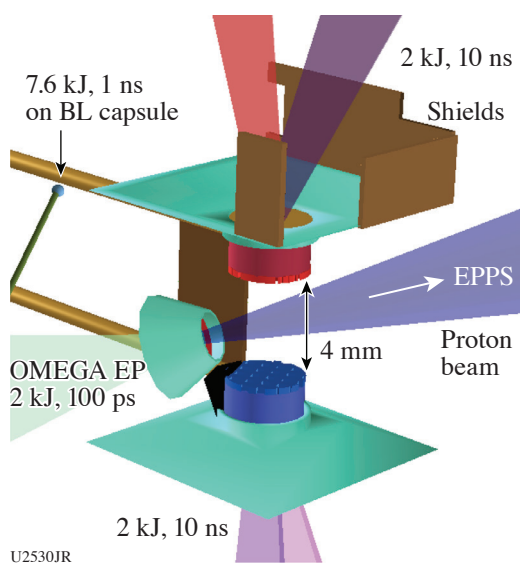


Figure 2
Experimental configuration. BL: backlighter.

The main diagnostics included an x-ray framing camera to measure self-emission from the turbulent plasma, proton radiography using a D^3He capsule irradiated with 17 OMEGA beams (450 J/beam, 1 ns) to probe the magnetic field structure of the plasma, and the EPPS to measure the energy spectrum of the TNSA proton beam. The EPPS was also equipped with a thin (<3-mm) RCF/CR39 stack in the front holder to measure the spatial profile of the beam. The streaked Thomson-scattering measurements indicate that the colliding plasma conditions are similar to previous experiments with electron temperatures of the order of 300 eV. The XRFC indicated fluctuations in plasma density in the collision region [Figs. 3(a)–3(c)] from which the density spectrum will be extracted. This can be compared with the spectrum of fluctuations in the plasma magnetic field, which will be extracted from the PRAD (proton radiography data) [Figs. 3(d) and 3(e)]. Qualitative study of the PRAD indicates modulated magnetic fields with small-scale structures visible at early times but not at later times. In addition to the displayed data, the EPPS indicates some energy-dependent transverse momentum imparted to the OMEGA EP proton beam as it transits the turbulent plasma.

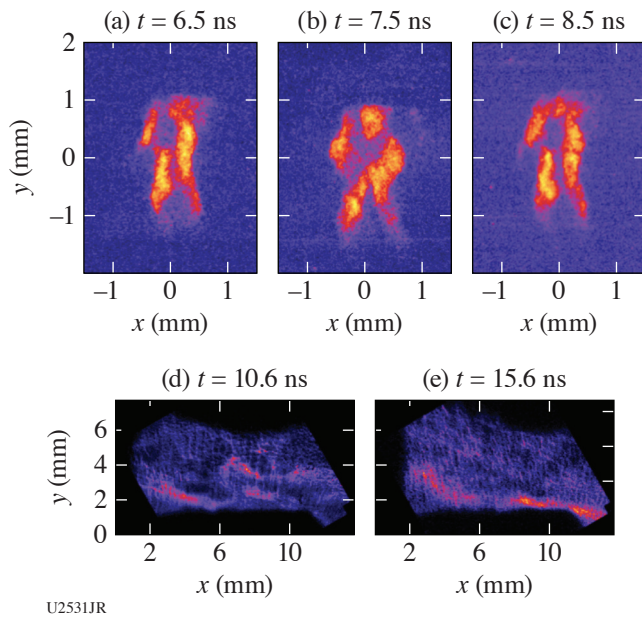


Figure 3

[(a)–(c)] Time series of XRFC images and [(d) and (e)] raw PRAD images where the brighter signal indicates higher proton flux. In both cases, time given is relative to nominal collision time of two ablation plasmas.

Inelastic Reactions of ^7Li from 14-MeV Neutrons Using an Inertial Confinement Fusion Platform

Principal Investigator: C. J. Forrest (LLE)

Co-investigators: J. P. Knauer, P. B. Radha, V. Yu. Glebov, O. M. Mannion, Z. L. Mohamed, S. P. Regan, T. C. Sangster, and C. Stoeckl (LLE); and W. U. Schröder (LLE and Dept. Chemistry and Physics, University of Rochester)

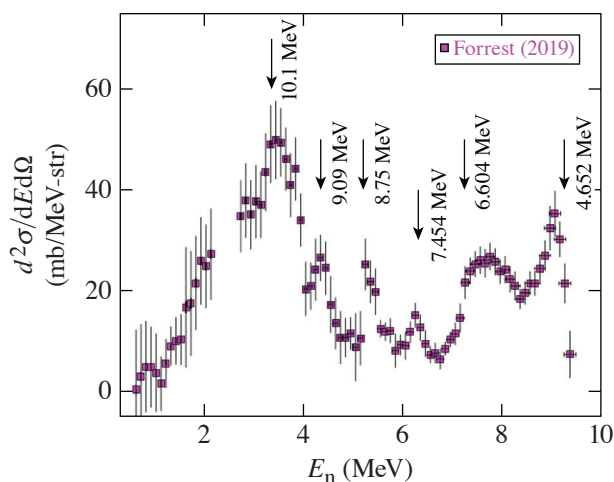
HEDLP (high-energy-density laboratory plasmas) is an established experimental platform that is used to address opportunities in a number of fields of scientific research.¹² Recently, HEDLP's generated on the OMEGA laser¹³ have been used to conduct basic nuclear science experiments. These facilities present viable and interesting alternatives to experimental accelerator-based platforms. In fact, primary yields are at the levels required to begin investigating fundamental nuclear reactions including neutron-induced breakup reactions of light nuclei. For these reasons, new fields of scientific exploration have been initiated for both nuclear interactions and high-energy-density plasmas.

Low-energy nuclear reactions involving light nuclei (for example, the breakup of a deuteron) represent one of the most attractive cases to study nucleon–nucleon interaction due to it being one of the simplest systems to evaluate.¹⁴ Experiments that inferred the double-differential cross section from the breakup of the deuteron have been compared to past measurements performed using accelerator-based platforms and *ab initio* calculations performed by A. Deluva, which are in good agreement with the recent measurements achieved on OMEGA.¹⁵ This measurement is currently the only data available that spans nearly the entire energy range from 1 to 10.5 MeV.

The production ^7Li nuclei play an important role in primordial nucleosynthesis, nuclear astrophysics, and fusion energy generation. Recent calculations using the no-core shell model with continuum (NCSMC) method are being applied to light nuclei to describe bound and scattering states such as ^7Be and ^7Li (Ref. 16). These calculations provide predictions for a resonance S-wave state for $^6\text{He} + p$ at a very low energy above the reaction threshold, which is relevant for astrophysics.

Recent experiments on OMEGA using the bright neutron source to irradiate ^7Li have measured the inelastic reaction cross sections as shown in Fig. 4. An enhanced peak at $E_n = 3.4$ MeV ($E_x = 10.1$ MeV) has been observed and might be the resonance from the $^6\text{He} + p \leftarrow$ state predicted using the NCSMC model. The next step is to submit another LBS proposal and to perform these experiments with both ^6Li and ^7Li to verify this resonance state.

This material is based upon work supported by the Department of Energy National Nuclear Security Administration under Award Number DE-NA0003856, the University of Rochester, and the New York State Energy Research and Development Authority.



U2481JR

Figure 4

The double-differential cross section has been measured using a high-yield 14-MeV neutron source incident on ${}^7\text{Li}$. Several of the known excited states are listed. The predicted state $E_x = 10.1$ MeV is from ${}^6\text{He} + p \rightarrow {}^7\text{Li}$ using the NCSMC analysis.

Turbulent Transport in Magnetized High-Energy-Density Plasmas

Principal Investigator: W. Fox (PPPL)

Co-investigators: D. Schaeffer, A. Bhattacharjee, and A. Spitkovsky (Princeton University); G. Fiksel (University of Michigan); and P. Knapp (SNL)

We have developed a new platform to study turbulent transport in magnetized laser plasmas on the OMEGA 60-beam laser. Anomalously fast diffusion of plasma across magnetic fields has long been recognized in magnetic fusion devices and laser plasmas. Microinstabilities driven by gradients in plasma parameters give rise to convective flow patterns on meso- to global scales, which leads to correspondingly enhanced diffusion coefficients. While some experiments have demonstrated aspects of anomalous transport in high-energy-density (HED) plasmas, many aspects remain unknown, and this physics is typically not included in magnetohydrodynamic (MHD) design codes for inertial confinement fusion (ICF). A key question when applying magnetic fields to HED plasmas is to understand the role of transport processes, in particular the processes that cause particles and field to mix and diffuse with respect to one another. These processes determine the time and space scales over which plasma heat can be effectively confined by the magnetic field. When plasmas are not created with embedded magnetic fields, diffusion is also a key step in “mixing” the field and plasma—a step that is important for creating large magnetized volumes of plasma for laboratory astrophysics experiments.^{17,18}

A particularly important example of magnetized confinement of HED plasma is the magnetized liner inertial fusion (MagLIF)¹⁹ approach to magneto-inertial fusion. The crucial questions of how well the hot plasma is insulated from the liner by the field and how ideally the field is compressed have not been addressed. These experiments also aim to help study the efficacy of magnetic insulation and flux compression that are essential to the scaling of the MagLIF concept.²⁰

During this LBS experiment we successfully carried out one shot day on OMEGA 60. We adapted a MIFEDS-based platform that we have previously used to study magnetic reconnection and shocks.^{17,18} To study turbulent transport, a plasma was ablated from a plastic target into a pre-existing magnetic field powered by MIFEDS. The interaction of the plasma with the field was diagnosed with 2-D proton radiography to map the magnetic-field topology. Protons measuring 3 and 15 MeV were produced by the implosion of a D^3He backlighter capsule and captured on CR-39. A Ni mesh was placed between the backlighter capsule and the plasma in order to make quantitative measurements of the magnetic-field deflection by tracking distortions in the mesh grid. Fiducial markings on the mesh allow for unambiguous identification of target chamber center (TCC). Image plates were also placed behind the CR-39 stack to capture x rays from the backlighter implosion. The resulting x-ray image provides another reference of the undistorted mesh for every shot. Additionally, local plasma parameters were measured with 2ω , spatially resolved Thomson scattering. The interaction of the laser plasma with the background field was measured for different laser energies and different target orientations relative to the field.

Figure 5 shows example proton radiography images, including a reference vacuum image [Fig. 5(a)] and 3- and 15-MeV images [Figs. 5(b) and 5(c), respectively] taken 12 ns after the laser plasma was ablated. With the plasma the mesh is heavily distorted in the 3-MeV image, indicating some turbulent structures. Figure 5(d) shows the path-integrated magnetic field $\int B \times dl$ from the 15-MeV reference (shot 92505) and plasma (shot 92515) images. The profiles taken across the midplane at two locations (above and below TCC) illustrate measurement noise. The vacuum profiles (blue curve) agree well with the expected signal from a model of the MIFEDS-generated field. The expansion of the plasma (red curve) creates a strong diamagnetic cavity, which evacuates most of the field. The results indicate that the cavity is still expanding or has recently stagnated. Furthermore, the measured field profiles, along with the density and temperature measured with Thomson scattering, confirm that these experiments are in a dimensionless regime similar to that of the MagLIF preheat conditions, with $\beta > 1$ and unmagnetized ions ($\nu_{ii}\omega_{ci} > 1$) and magnetized electrons ($\nu_{ei}\omega_{ce} > 1$), where $\nu_{e,i}$ are the collision frequencies and $\omega_{ce,i}$ are the gyrofrequencies. Additional measurements in an upcoming shot day will explore later times when the cavity starts collapsing.

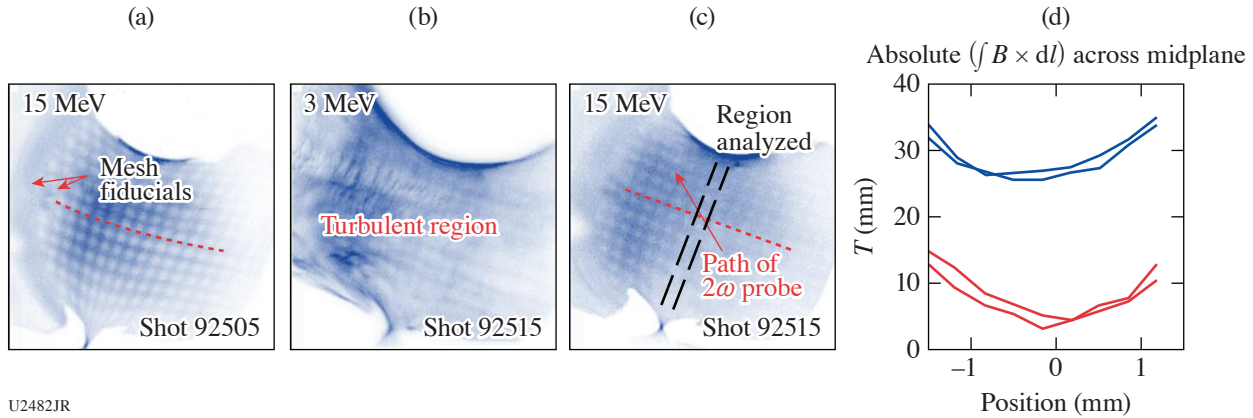


Figure 5

Example proton radiography images. (a) Reference image taken in vacuum. The mesh pattern is distorted by the MIFEDS magnetic field, but it can be referenced against fiducials. (b) A 3-MeV image taken 12 ns after the laser plasma is ablated. (c) A 15-MeV image taken on the same shot as (b). The mesh pattern is still visible, allowing for quantitative analysis. (d) Comparison of measured path-integrated magnetic-field profiles from the reference (blue curve) and plasma (red curve) images. The region analyzed for both images is shown in (c).

Investigating Giant Impacts Between Rocky Planets with High-Pressure Melting and Shock Equation-of-State Measurements on Complex Silicates—SilicateEOS-EP-19

Principal Investigators: D. E. Fratanduono and M. Millot (LLNL)

Co-investigators: B. Chidester,* D. Spaulding, and S. Stewart, (University of California, Davis); J. Li (University of Michigan); and J. Townsend* (SNL)

Graduate students: E. Davies and K. Amodeo (University of California, Davis)

*Postdoc

We conducted experiments to investigate the melting behavior and pressure–density–temperature (P – ρ – T) shock equation of state (EOS) and document bonding changes in hot liquid states of complex silicate minerals using ultrafast velocimetry and pyrometry measurements up to 2 TPa. Our goal is to address one of the most puzzling questions in planetary sciences: How did energetic collisions in the early solar system result in the physical structures and chemical compositions of the terrestrial planets? We also wish to document the structure and melting processes of multicomponent liquids, which is fundamental to both planetary sciences and HED physics.

Because it is necessary to constrain the thermodynamic response of the planet-forming materials to understand the dynamics of sub-giant and giant collisions and to examine the potential for chemical equilibration between the target and the impactor, we

concentrated our effort on natural samples from the olivine $[(\text{Mg,Fe})_2\text{SiO}_4]$ and orthopyroxene $[(\text{Mg,Fe})\text{SiO}_3]$ mineral families, which constitute the majority of the silicate mantles of the terrestrial planets (e.g., Earth, Mars) by volume.

This shot day completed 14 shots on the OMEGA EP laser, alternating beams to increase the shot rate. Velocity interferometry and optical pyrometry with decaying shocks (Fig. 6) measured the shock temperature and the intersection of the Hugoniot with the melting curve for two minerals: olivine $[(\text{Mg}_{90}\text{Fe}_{10})_2\text{SiO}_4]$ and bronzite $[(\text{Mg}_{90}\text{Fe}_{10})\text{SiO}_3]$. After detailed analysis and upcoming complementary experiments in FY20, these data will be used to develop improved EOS models for hydrodynamic simulations of impact events and interior structure models. In particular, the olivine data will be compared to previous experiments at the Omega Laser Facility on the pure end-member mineral forsterite: $(\text{Mg}_2\text{SiO}_4)$ reported in Ref. 21. The bronzite data will complement the previous work on MgSiO_3 enstatite described in Ref. 22.

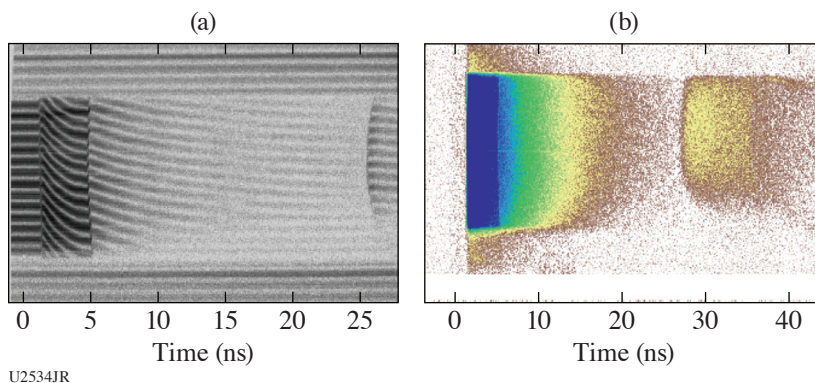


Figure 6

(a) Example active shock breakout (ASBO) and (b) streaked optical pyrometer (SOP) data for the SilicateEOS-EP-19 Campaign showing a decaying shock traveling through the multilayer package to reveal the optical and thermodynamic properties of bronzite in the Mbar range.

Phase Transformation Kinetics—Strain Rate Tuning of the Peierls Distortion in Ramp-Compressed Body-Centered Tetragonal Tin

Principal Investigators: M. Gorman and R. Smith (LLNL)

The goal of the SnKinetics-19A/B/C experiments on OMEGA was to develop a ramp-compression platform to determine the crystal structure of tin (Sn) up to 70 GPa at several different compression rates. These observations will be compared to shock and static measurements on Sn and are expected to confirm a previously unreported mechanism responsible for altering crystal structure evolution under dynamic compression conditions.

In the target design shown in Fig. 7 we use a plasma piston design²³ to ramp compress a 6- μm -thick Sn layer, which is directly coated onto a LiF window. To minimize the heat transfer from the plasma to the Sn sample, we incorporate a 6- μm -thick preheat shield. A 50- μm -thick, 50-g/cm³ additive manufactured foam (AMFoam) layer is used to temporally shape the ramp and pressure hold profile experienced by the Sn layer.²⁴ The OMEGA VISAR (velocity interferometer system for any reflector) active shock breakout (ASBO) measures the Sn/LiF particle velocity from which the sample pressure as a function of time can be determined.²⁵ These experiments combine nanosecond x-ray diffraction²⁵ and ramp compression to dynamically compress and determine the crystal structure of Sn/LiF to peak pressures within the 10- to 70-GPa range. Using the OMEGA powder x-ray diffraction image-plate (PXRDIIP) diagnostic,²⁵ the compressed Sn sample is probed with a 1-ns He_α x-ray source to determine crystal structure at a well-defined sample pressure (VISAR). Figure 8 shows an example of the data, with information on the high-pressure body centered cubic (bcc) phase of Sn. Also observed are peaks from the ambient pressure W pinhole that serve to calibrate diffraction angle.

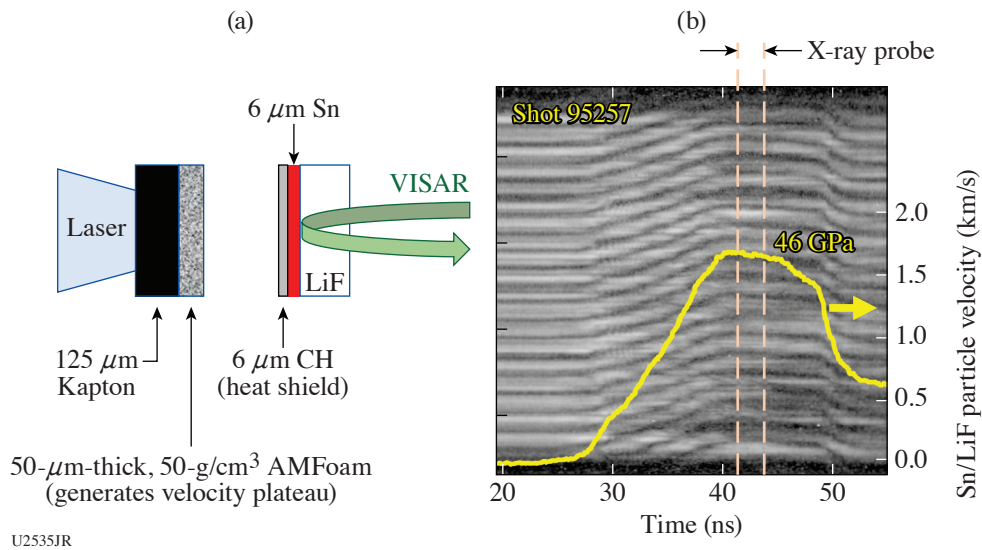


Figure 7
 (a) Target design for ramp-compression experiments of Zr using the OMEGA laser. (b) Raw VISAR data with extracted Sn/LiF particle velocity profile. As indicated a Cu He α x-ray source is timed to probe the sample at peak compression. For shot 95257 (as shown) the peak sample pressure for Sn is 46 GPa.

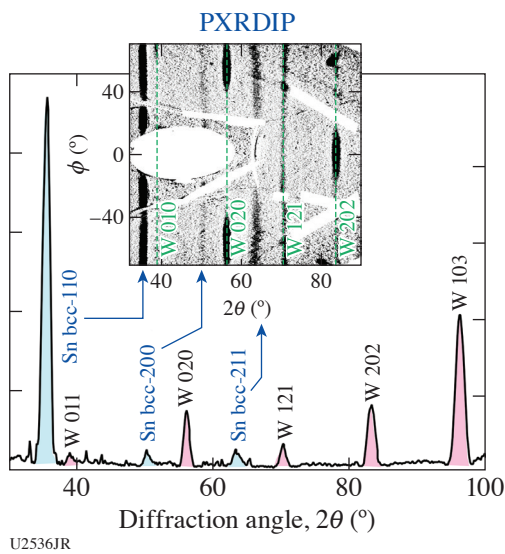


Figure 8
 Diffraction pattern for ramp-compressed Sn up to peak pressures of 46 GPa. Here the Sn bcc phase is observed along with the ambient pressure W-pinhole calibration peaks.²⁵

Implementation of a Broadband Optical Spectroscopy Diagnostic for OMEGA EP

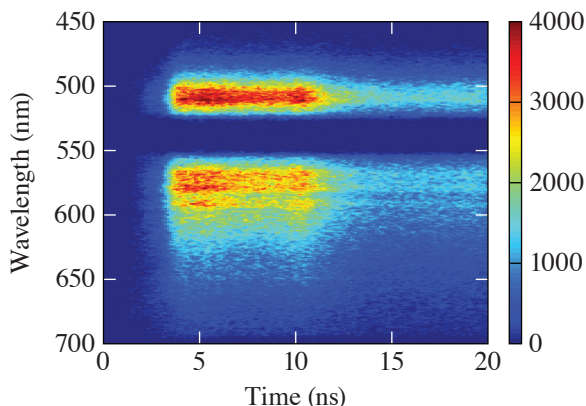
Principal Investigator: B. J. Henderson (LLE and Dept. of Physics and Astronomy, UR)

Co-investigators: J. R. Rygg (LLE, Dept. of Physics and Astronomy, UR); J. Katz, C. Sorce, J. Kendrick, A. Sorce, T. R. Boehly, and M. Zaghoo (LLE); and G. W. Collins (LLE and Dept. of Mechanical Engineering, UR)

Matter, when subject to extreme pressures and temperatures, can experience significant changes in optical, structural, and electronic properties. These transitions often manifest themselves through changes in optical transport properties, the most readily observable being reflectance and absorption. Experiments on OMEGA EP have sought to measure reflectance with the monochromatic VISAR diagnostic.²⁶ While single-wavelength reflectivity measurements can be used to identify phase transitions, they lack the required spectral dependence to determine properties such as plasma frequency and band gap. Our work

shows (1) a proof of principle for recovering a reflected broadband signal from compressed aluminum and (2) the system's ability to accurately measure temperature in high-pressure shocks.

Aluminum's ambient band structure contains parallel bands that preferentially absorb near 1.5 eV (~825 nm). Under the effects of compression, the energy gap between these bands expands, shifting interband absorption to higher photon energies with increasing pressure.²⁷ To examine this high-pressure behavior, we submitted an LBS proposal to investigate electronic structure changes in matter at extreme conditions. Figure 9 shows a reflected broadband signal from an isentropically compressed Al–LiF interface. The broadband probe is generated by a CH–quartz–SiO₂ foam target and redirected to the back side of the sample via an in-chamber optical train. Analysis of these results is still ongoing.



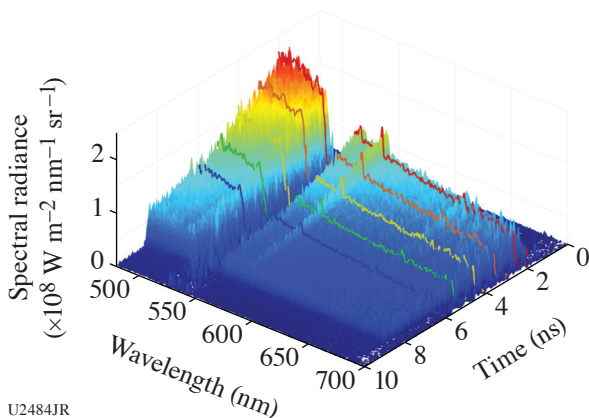
U2483JR

Figure 9

Streak image of a reflected broadband signal from shot 30375. The back-lighter is driven at 2 ns, the shock enters the quartz pusher at 3.5 ns, and the backlighter achieves a temporally flat brightness profile at 6 ns in the SiO₂ foam. A significant decrease in signal observed at 11 ns is due to changes in optical properties in the compressed target.

Additionally, this diagnostic was proposed as a powerful tool for high-accuracy temperature measurements in strongly shocked materials. For systems with unknown shock pressure–temperature scaling, quartz is the typical reference for new measurements. The quartz *P–T* scaling for shock compression has been reported²⁸ and is widely used in many HED experiments. The uncertainty in this scaling remains quite large, however, primarily due to the use of spectrally integrating diagnostics to measure shock brightness. With spectral resolution, we can directly observe the Planck's law scaling of thermal emission with temperature. Figure 10 shows the recorded emission spectrum of a decaying shock in quartz. This data will be used to refine quartz's ability to function as a temperature standard in future HED experiments.

This material is based upon work supported by the Department of Energy National Nuclear Security Administration under Award Number DE-NA0003856, the University of Rochester, and the New York State Energy Research and Development Authority.



U2484JR

Figure 10

Emission spectrum from a decaying shock in quartz from shot 30378. Single-time lineouts (many colors) are fit with a Planck's Law function to determine the temperature. "Spikes" and "troughs" in the spectrum are due to filters in the VISAR–SOP relay.

Developing Inverted-Corona Fusion Targets as Neutron Sources

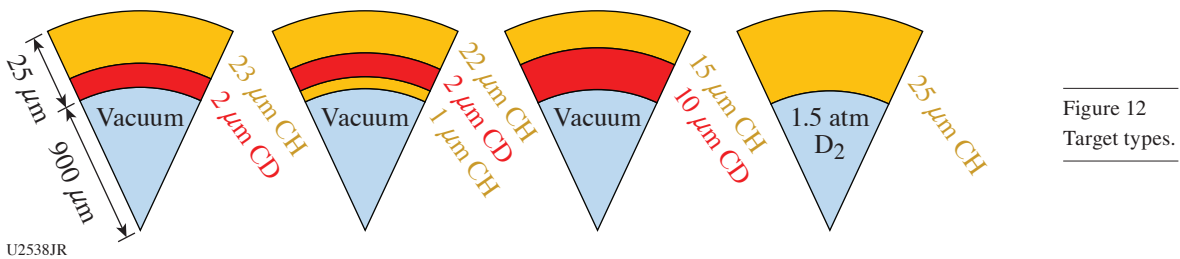
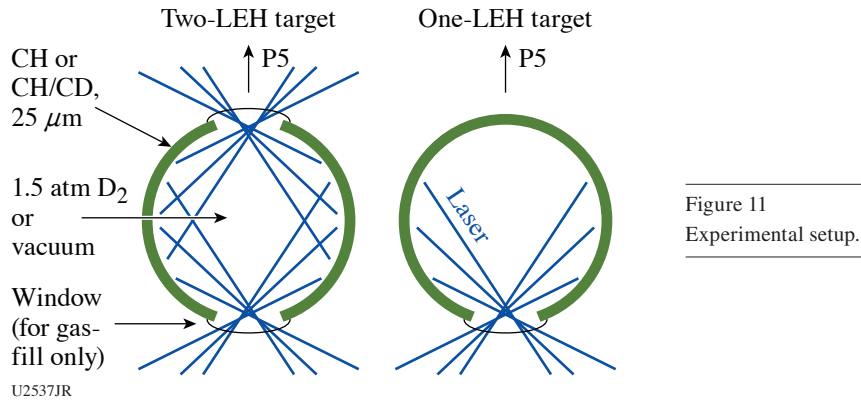
Principal Investigators: M. Hohenberger (LLNL) and S. Glenzer (SLAC)

Co-investigators: N. B. Meezan and A. J. Mackinnon (LLNL); and M. Cappelli (Stanford)

Graduate students: W. Riedel (Stanford); N. Kabadi (MIT); and F. Treffert (SLAC)

These experiments explored the feasibility of inverted-corona targets as fusion-neutron sources for HED applications. In inverted-corona targets, laser beams directly ablate a layer of fusion fuel on the inner surface of a target, e.g., a CD-lined capsule.^{29,30} As the ablative flows converge at the target’s center, the plasma particles transition from long-range interactions to collisional stagnation, heating the ions and generating fusion reactions. The fusionable material may also be provided as a gas fill, where, similar to an exploding pusher, the laser-driven ablation launches a centrally converging shock into the gas, thereby heating it to fusion conditions.

The experimental setup is shown schematically in Fig. 11. Target capsules with a 1.8-mm inner diameter and 25- μ m-thick walls had one (or two) laser entrance holes (LEH’s) and were laser irradiated by 19 (or 39) beams with 1-ns square pulses at up to 500 J/beam. CH capsules with 1.5 atm of D₂-gas fill were fielded, as well as vacuum, CD-lined CH capsules with varying liner thickness or liner depth (see Fig. 12).



Generally, 2-D *HYDRA* calculations predicted a linear scaling of yield with incident laser energy, while the 1- or 2-LEH configuration had little performance impact. With a calculated yield of up to $\sim 10^{11}$ neutrons at 18 kJ of incident energy, *HYDRA* 2-D simulations predicted the highest yields for the gas-filled capsules. For the vacuum targets, *HYDRA* predicted most of the D–D fusion to occur in the stagnating ablation plasma from the innermost 1- μ m layer of CD liner, with little increase in yield beyond that thickness, and peak neutron yield of $\sim 5 \times 10^{10}$ at 18 kJ of incident energy. Recessing the CD liner 1 μ m into the wall decreased calculated yield by $>30\times$.

This is in contrast to the experimental neutron yields, which are plotted in Fig. 13 on a logarithmic scale and as a function of laser energy. While these data also follow a linear trend with energy, the experiments generally underperformed compared to the simulations, with Y/Y_{2-D} between $\sim 5\%$ to $\sim 15\%$. Furthermore, the experimental data exhibit a strong dependence of yield on liner thickness, with an $\sim 15\times$ increase in yield from the $2\text{-}\mu\text{m}$ (circles) to the $10\text{-}\mu\text{m}$ CD liner (triangles), with the latter giving the highest performance of $\sim 1.5 \times 10^{10}$. This indicates significant mixing in the ablative plasma, confirmed by the minor drop in yield for the recessed $2\text{-}\mu\text{m}$ CD liner (diamonds).

With a detailed data analysis in progress, these experiments support promising applications; e.g., neutron radiography at the NIF requiring a total yield of $\sim 10^{14}$ should be possible using a DT-gas-filled, single-LEH target and few-hundred-kJ driver energies.

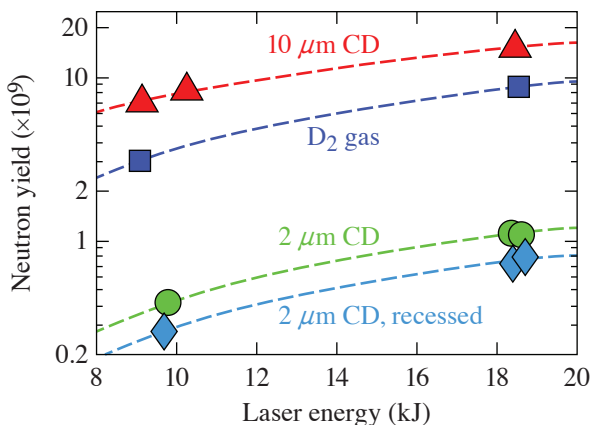


Figure 13
Neutron yields.

U2539JR

Characterizing Pressure Ionization in Ramp-Compressed Materials with Fluorescence and Absorption Spectroscopy

Principal Investigators: S. Jiang and Y. Ping (LLNL)

Co-investigators: A. Lazicki, P. Sterne, P. Grabowski, H. Scott, R. Smith, R. Shepherd, B. Bachmann, and J. Eggert (LLNL); and S. B. Hansen (SNL)

This pressure ionization campaign comprised a half-day on OMEGA and one day on OMEGA EP during FY19. Following the previous FY18 campaign, which for the first time provided a direct benchmark between various isolated-atom and average-atom ionization models by measuring K-shell fluorescence emission of Co, the FY19 campaign extended the measurement to study a possible K-edge shift and began an investigation of L-shell emission lines.

On OMEGA, we have measured the K edge of compressed Co as a function of density. A schematic of the experimental setup is displayed in Fig. 14(a). The high pressure in Co was achieved by ramp compression using the long-pulse drivers to keep the temperature low during the compression process. The pulses were designed to mimic the drive used on OMEGA EP during the FY18 campaign. The pressure history was characterized with on-shot VISAR measurements. Under two different drive energies, 1500 J and 6600 J, the sample reached $1.5\times$ and $2.1\times$ compression, correspondingly. We used a foil x-ray backlighter and measured the absorption spectra using a high-resolution spectrometer IXTS. No obvious Co K-edge shift was observed [Fig. 14(b)], which is consistent with the prediction of average-atom models but disagrees with the commonly used isolated-atom models. We were also able to measure the EXAFS [Fig. 14(c)] to confirm low temperature in compressed Co.

On OMEGA EP, the L-shell fluorescence emission of Sn was observed using the IXTS spectrometer configured with a lower-energy PET (pentaerythritol) crystal. In this experiment a short-pulse laser beam irradiated a secondary Be target that was directly attached to a Sn foil. The hot electrons generated by the laser-Be interaction could transport to the Sn layer and induce fluorescence. Sn L_β spectra with different Be thicknesses are shown in Fig. 15. The L_β line shifts to higher energy with increasing

temperature (thinner Be). Detection of this L_{β} line under compression proved more challenging due to backgrounds generated by the long-pulse beams but is promising for future work.

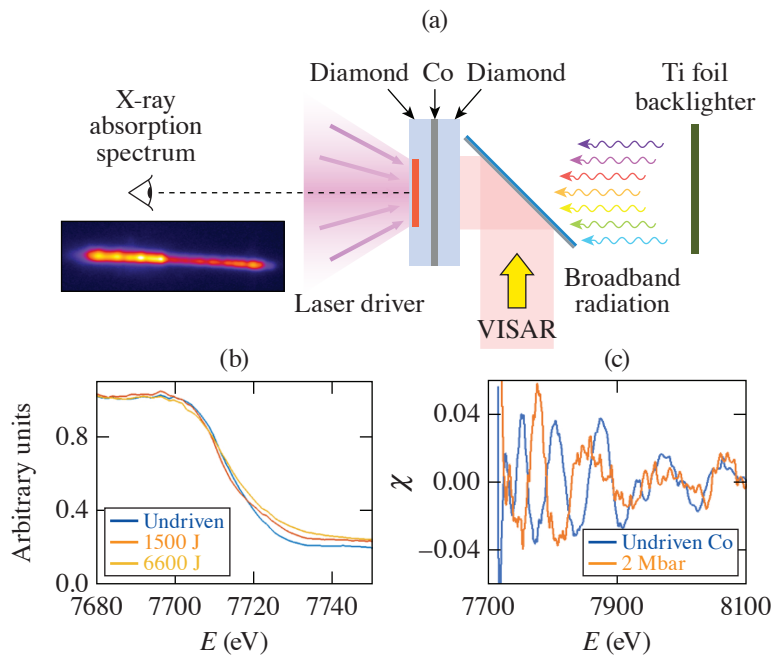


Figure 14
(a) Experimental schematic and [(b) and (c)] results on OMEGA.

U2540JR

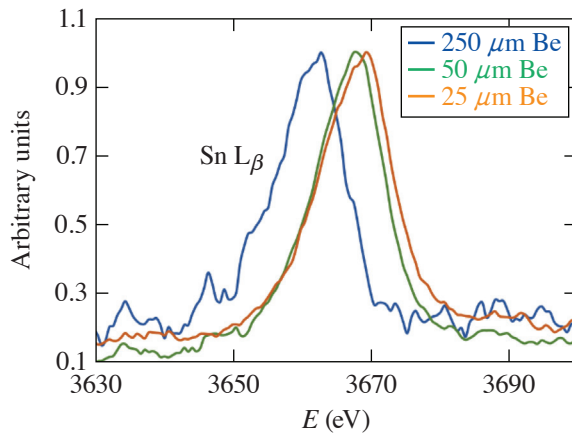


Figure 15
Sn L_{β} fluorescence spectra.

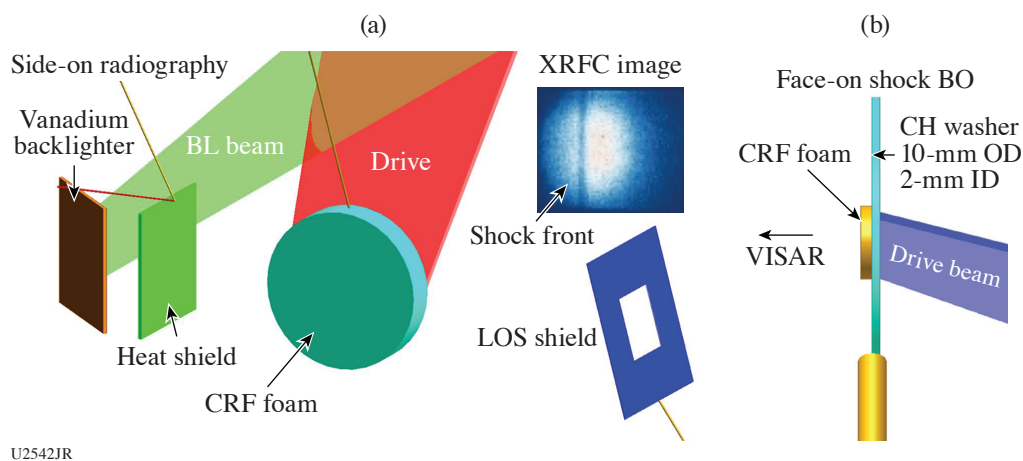
U2541JR

Shock Trajectory in Low-Density Carbonized Resorcinol-Formaldehyde Foams for the Landau–Darrieus Instability

Principal Investigator: S. F. Khan (LLNL)

Co-investigators: A. Casner, L. Masse, L. Ceurvorst, T. Goudal, D. Martinez, and V. A. Smalyuk (LLNL)

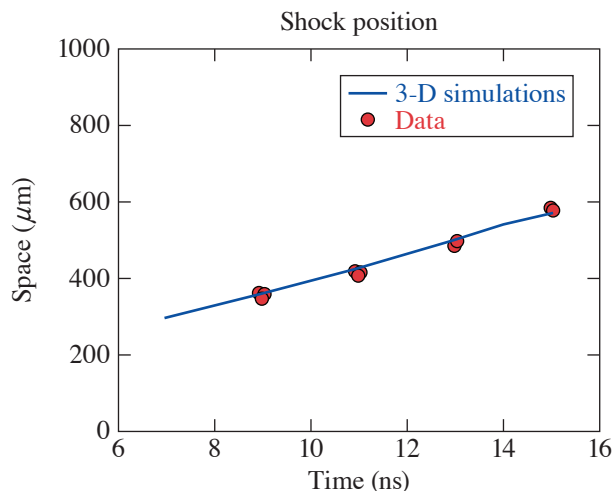
The objective of these OMEGA EP experiments is to measure the shock trajectory into driven carbonized resorcinol-formaldehyde (CRF) foams in order to select the optimum material density and drive laser intensity for NIF Discovery Science experiments to study the Landau–Darrieus instability (LDI) in laser ablation. Two CRF densities were tested, nominally 50 mg/cm³ and 100 mg/cm³. The tested drive laser intensities were 5×10^{12} W/cm², 1×10^{13} W/cm², and 2×10^{13} W/cm². The shock trajectory was tracked using side-on radiography and the shock breakout was measured using VISAR face-on (see Fig. 16). The side-on radiography was imaged onto an x-ray framing camera using a V backlighter. The shock was clearly visible in most



U2542JR

Figure 16
Experimental layout with primary measurements: (a) side-on radiography and (b) face-on shock breakout using VISAR.

of the frames and the shock breakout was clear. For the 100-mg/cm^3 CRF foam driven at $5 \times 10^{12} \text{ W/cm}^2$, side-on radiography measured a velocity of 25 to 30 km/s, the shock breakout measurement gave a velocity of 21 km/s, while initial 2-D simulations gave 16 km/s. However, considering these results, 3-D simulations (see Fig. 17) were performed with actual laser spot size and incidence angle that show a much better agreement. For the NIF Discovery Science experiments, the 100-mg/cm^3 density was chosen to be driven with an intensity of $1.25 \times 10^{12} \text{ W/cm}^2$. We used a lower laser intensity to observe the LDI before the shock breakout and Rayleigh–Taylor instabilities were generated.



U2543JR

Figure 17
Shock position as a function of time.

Development of the New Forward–Backward X-Ray Diffraction Diagnostic

Principal Investigator: A Krygier

Co-investigators: C. E. Wehrenberg and A Gleason (SLAC); and H.-S. Park and J. H. Eggert (LLNL)

This LBS experiment, as shown in Fig. 18, was the first effort to collect simultaneous transmission and reflection diffraction from a sample driven to high pressure with the new forward–backward x-ray diffraction (FBXRD) diagnostic. By using two monochromatic x-ray sources, we simultaneously probed the sample in multiple geometries, maximizing coverage of the range of angles between the diffraction plane and applied stress direction. This capability will be able to constrain the *in-situ* strain anisotropy induced by material strength in a polycrystalline sample.

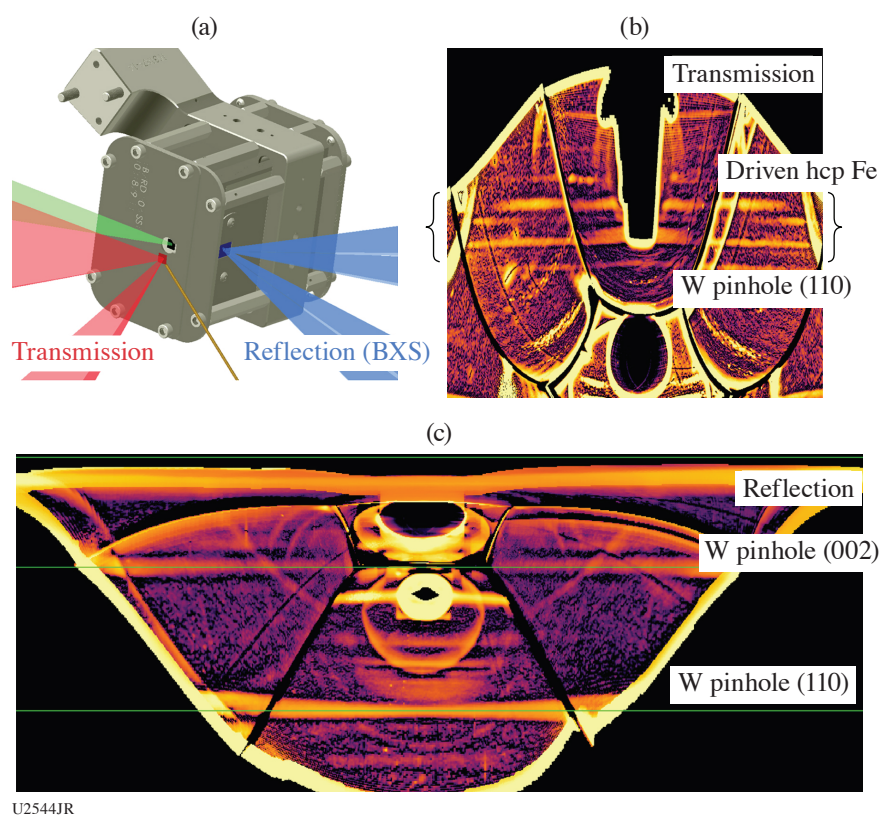


Figure 18

(a) Experimental setup; (b) driven x-ray diffraction in the transmission geometry showing high-pressure Fe hcp phase reflections; and (c) reflection geometry x-ray diffraction. The bright lines shown are from the W pinhole.

Many of the shots on this campaign were dedicated to optimizing the backlighter, shielding, and pinhole configuration. We performed a scan of reflection backlighter laser illumination energies and spot sizes using diffraction quality as the ultimate judge of each configuration. We found that a range of conditions produces high-quality diffraction. We also tested several conical shielding configurations for the backward x-ray scattering (BXS) reflection diffraction setup, including tungsten, stainless steel, and plastic; tungsten worked best. We have identified several sources of background signal that confound a full interpretation of the diffraction signal.

Time-Resolved Measurement of Germanium L-Shell Emission Using a Buried Layer Platform

Principal Investigator: E. V. Marley (LLNL)

Co-investigators: D. Bishel, M. Frankel, Y. Ehrlich, Z. Shpilman, M. B. Schneider, G. E. Kemp, R. F. Heeter, M. E. Foord, D. A. Liedahl, K. Widmann, and J. Emig (LLNL)

This campaign was designed to measure the emitted L-shell germanium spectra from a well-characterized and uniform plasma for comparison to atomic kinetic models. Recent studies have shown a discrepancy between atomic kinetic models and high-Z M-shell spectral data. This study was conducted to test the accuracy of models for L-shell emission.

Planar, buried-layer targets were illuminated equally on both sides (Fig. 19) to heat the sample. The sample used in the campaign was a 2000-Å-thick Ge/Sc mixture designed to burn through completely before the end of the laser pulse, providing uniform plasma conditions to measure the L-shell emission of the germanium. The samples were buried between two 5- μm -thick layers of Be, which acted as an inertial tamp slowing the expansion of the sample.

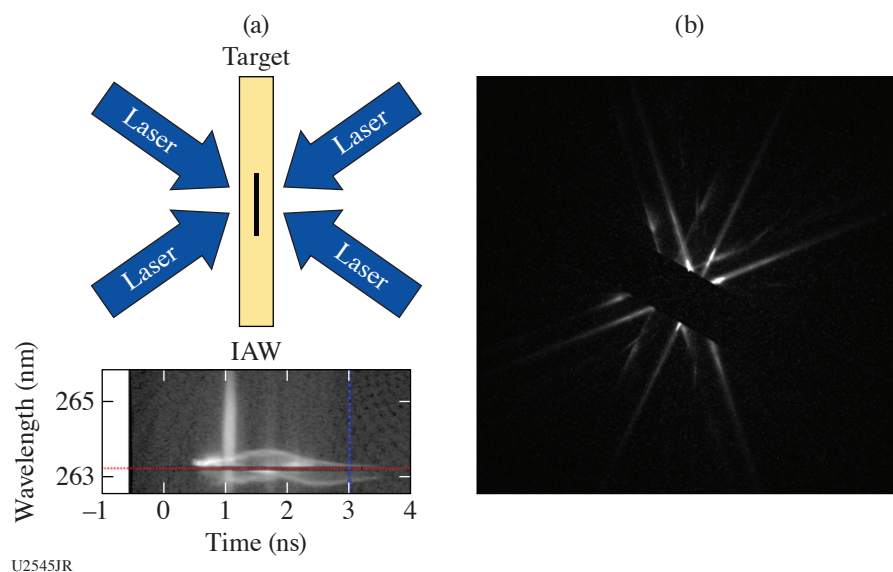


Figure 19
 (a) Experimental configuration; (b) Thomson-scattering data of shot 94085; and (c) TGS data of Ge and Sc L-shell spectra.

Time-resolved 2-D images of the target's x-ray emission, viewed both face-on and side-on, were recorded using pinhole cameras coupled to framing cameras. The 4ω probe beam and Thomson spectrometer were also used to measure the scatter off the electron and ion acoustic features [see Fig. 19(b)]. A new filter package was used during the campaign to filter out the self-emission and unconverted light, providing high-quality scattering data. The K-shell spectra from the Sc were used to determine the electron temperature of the plasma. The time-resolved spectra were recorded using a crystal spectrometer coupled to a framing camera. A crystal spectrometer was used to record the Ge L-shell emission, also time resolved. All of the framing cameras, those used for imaging as well as those used for spectroscopy, were co-timed so the plasma conditions could be determined for the measured Ge L-shell emission.

The Soreq transmission grating spectrometer (TGS), as part of the ongoing LLNL/Soreq collaboration, was used to record the absolutely calibrated time-integrated germanium and scandium L-shell emission onto an x-ray charge-coupled device.

A single pulse shape was used during the campaign: a 3.0-ns square pulse with a 100-ps picket arriving 1 ns before the main pulse. A complete (all six diagnostics, correctly timed and pointed) set of data was recorded during the campaign at temperatures of ~ 2 keV.

A Journey to the Center of Uranus and Neptune: Using X-Ray Diffraction to Unravel the Atomic Structure of New Solid and Superionic Ices at Multimegabar Pressures

Principal Investigators: M. Millot and F. Coppari (LLNL)

Co-investigators: D. E. Fratanduono and S. Hamel (LLNL); S. Stanley (Johns Hopkins University); and M. Bethkenhagen (Postdoc, Rostock University, Germany)

We conducted an OMEGA EP one-day campaign to investigate the structure and equation of state of solid and superionic water at Uranus's and Neptune's deep interior conditions with a combination of ultrafast x-ray diffraction and optical diagnostics using new laser dynamic compression techniques.

This work expands on our recent discovery of superionic water ice at the Omega Laser Facility (LBS Campaign on Extreme Chemistry, FY13) reported in Ref. 31 and the subsequent discovery of a new superionic water ice XVIII (LBS Campaign on

SolidWater, FY14 described in Ref. 32). Superionic ices, a new exotic state of matter, are characterized by fluid-like diffusing hydrogen ions (protons) within a solid lattice of oxygen ions, which could dominate the interiors of icy giant planets such as Uranus, Neptune, and their extra-solar cousins.

We successfully commissioned the new platform for x-ray diffraction of initially liquid samples on the OMEGA EP laser and collected excellent quality data on eight system shots using two UV beams to compress the water sample layer and two UV beams to generate an x-ray source flash for the x-ray diffraction measurement (Fig. 20). Preliminary analysis suggests that the use of longer pulse duration allowed us to explore lower-temperature compression paths to search for predicted new phases of solid ices of pure water.³³

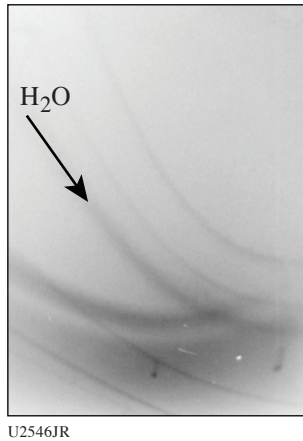


Figure 20
Raw PXRDIP data showing the successful observation of x-ray diffraction from Mbar water ice on OMEGA EP.

We also explored higher-temperature compression paths that reproduce the pressure–temperature conditions inside Neptune and Uranus to constrain the melting line near 1 Mbar and document the atomic structure and transport properties of pure water at these conditions.

Changes in the Electronic Structure of Dense, High-Temperature Matter

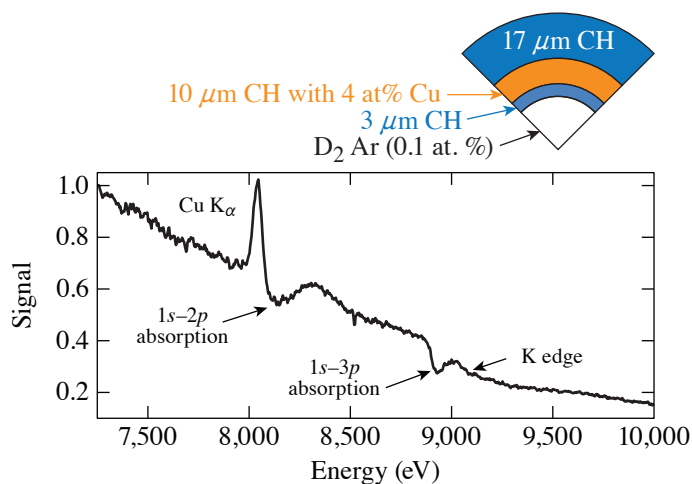
Principal Investigators: P. M. Nilson and S. X. Hu (LLE); and S. B. Hansen (SNL)

Graduate Students: D. A. Chin, J. J. Ruby (LLE)

The goal of this campaign is to test atomic-scale models that are used to estimate changes in the electronic structure of compressed materials. How atomic physics may be altered in these conditions is of fundamental importance to the study of stellar interiors, planetary cores, and inertial fusion. To measure detailed x-ray absorption features and fluorescent line emission from dense, high-temperature matter, a self-backlit, spherical-implosion platform is being developed on the OMEGA Laser System.

The experiment uses a 30- μm -thick plastic shell that contains a metal-doped layer. The inset of Fig. 21 shows the target design. The spherical target has three layers: a 17- μm CH ablator, a 10- μm CH layer doped with 2 or 4 at. % Cu, and an inner 3- μm CH layer. A slow, moderate-convergence implosion is used to assemble the material under study and to backlight its properties using continuum emission generated in the core at bang time. The target is driven by direct laser ablation using a 27-kJ, 1-ns drive. To provide information on the imploded-core conditions, the target contains a 20-atm D₂ Ar (0.1 or 1 at. %) fill.

Figure 21 shows an example of time-integrated x-ray emission and absorption spectrum from these experiments. The data show the Cu K-edge shape and spectral shift, in addition to the Cu K α emission and resonant 1s–3p and 1s–2p self-absorption features. These x-ray spectroscopic features were time resolved in the experiment using a streaked x-ray spectrometer (not shown). Detailed analysis of the simultaneous time-integrated and time-resolved x-ray emission and absorption spectra is underway for comparison with model predictions. The ultimate goal is to use these data to constrain the ionization balance and investigate the importance of density effects on the conditions that are generated. Future work will apply these techniques to both closed- and open-shell systems.



U2485JR

Figure 21
 Example of time-integrated x-ray absorption features and fluorescent line emission from a laser-driven implosion containing a Cu-doped layer. The target design, shell composition, and core fill are shown in the inset.

The Effects of the Plasma Geometry on the K-Shell Spectrum of Mid-Z (21–26) Ions

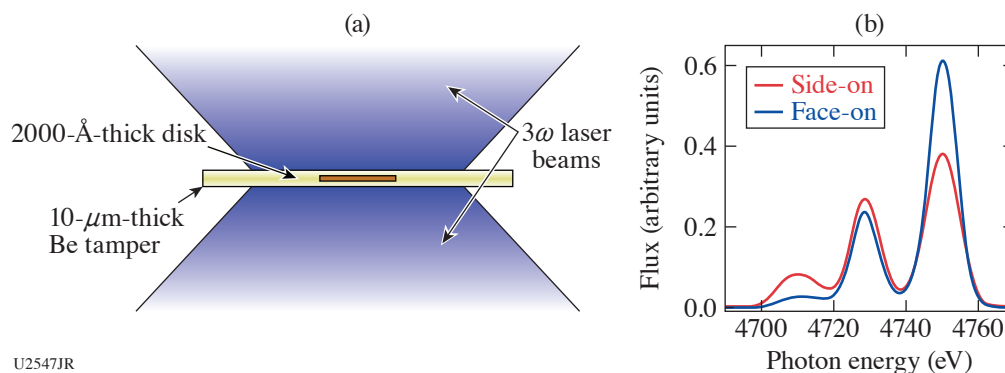
Principal Investigator: G. Pérez-Callejo (student, University of Oxford)

Co-investigators: E. V. Marley,* M. B. Schneider, G. E. Kemp, M. E. Foord, R. F. Heeter, D. A. Liedahl, G. V. Brown, and J. Emig
 Students: D. Bishel (LLE)

*Postdoc

This campaign was designed to measure the K-shell spectra of mid-Z atoms in well-defined and uniform plasmas in order to characterize how the flux from optically thick lines depends on the geometry of the plasma. This idea has been studied mainly in astrophysics, but the aim of this study was to take advantage of said geometric effects for characterizing the plasma conditions in dot spectroscopy experiments on the NIF. On two shot days, planar buried layer targets were illuminated evenly on both sides to heat the sample [Fig. 22(a)], which consisted of a Ti-only disk for the first shot day, and were changed to a 1:1 mixture of Sc and V for the second shot day. This change minimized the presence of Be impurities in the spectra, as well as the optical depth of the disk. The sample was tamped on both sides by 5- μm -thick layers of Be to slow the sample's expansion and provide radial confinement to maintain its cylindrical shape.

In both shot days, the pulse shape was kept the same, a 2.7-ns square pulse to maintain the maximum possible uniformity. A complete (all six diagnostics, correctly timed) set of data was recorded during the campaign at temperatures ~ 1.5 keV. The initial data look promising.



U2547JR

Figure 22
 (a) Experimental configuration and (b) time-resolved Ti H_{α} spectra with data inset at 2.7 ns of shot for both face-on and side-on configurations.

Time-resolved 2-D images of the targets' x-ray emission viewed both face-on and side-on were recorded using gated pinhole imagers. The K-shell spectra were measured in four time windows using crystal spectrometers, with focus on the He α complex [Fig. 22(b)]. The temperature of the plasma was determined from the optically thin spectra lines using a genetic algorithm approach. For the second day, the ratio of isoelectronic lines provide a more accurate measurement of the temperature. The plasma density was obtained from the measured size of the plasma at every time by imposing a conservation of particles condition.

On the first shot day, a high-resolution double-crystal spectrometer with spatial resolution was fielded on OMEGA to study possible uniformities in the plasma. On the second shot day, this spectrometer was replaced with a streak camera to study the heating processes of the Sc and V in a continuous manner. In both shot days, a TGS from the Soreq Institute, Israel, was fielded to check, against hydrodynamic simulations, how the plasma was being heated as the laser burned through the Be tamper.

Viscosity Measurements Using Tracer Particles

Principal Investigator: J. Shang (Dept. Mechanical Engineering, University of Rochester)

Co-investigators: D. N. Polsin, H. Aluie,* D. Kelley,* J. R. Rygg, R. Betti,* J. F. Myatt, J. Zhang,* R. W. Short, A. V. Maximov,* W. Seka, D. H. Froula,[†] D. H. Edgell, D. T. Michel, and I. V. Igumenshchev (LLE); A. Gleason (SLAC National Accelerator Laboratory and Stanford University); and D. E. Hinkel, P. Michel, and J. D. Moody (LLNL)

*Also Dept. Mechanical Engineering, University of Rochester

[†]Also Dept. of Physics and Astronomy, University of Rochester

Most numerical models in HED applications such as ICF do not include the viscosity for materials being simulated.^{34,35} Yet, it is well known that viscosity plays an important role in the evolution of hydrodynamic instabilities and the mixing between materials, especially at early times at scales smaller than 100- μ m diameter. Our objective was to measure viscosity in an HED polymer, such as CH, which is commonly employed in target fabrication for ICF and basic science experiments. In this experiment, we aimed to shock-compress the CH and track the movement of small, high-Z particles embedded in the CH over time. The viscosity plays a role in how well a particle tracks the surrounding fluid and can be inferred by comparing trajectories of particles of different sizes and/or density after a shock has passed.

Our target bulk was composed of particle-seeded epoxy; as a CH material, we have a reasonable understanding of how it will behave under shock compression, and high-Z particles (Ti, W) can be introduced before it cures. The final targets for this campaign have manually positioned particles, with their positions consistent between targets within 50 μ m. Ideally, the bulk medium would be homogeneous; however, to position the particles reproducibly, a support structure of amorphous silica supports the epoxy layer; because of the density difference between the epoxy and the silica, this likely produced a nonuniform shock that will affect the particle dynamics.

The experiments used area backlighting to track particle motion over four time slices as recorded on an XRFC (Fig. 23). Here, two laser beams irradiated a plastic ablator at the front of the target using 1100- μ m distributed phase plates, driving a shock through the material. As the CH started to flow during the shock process, the idea was that the embedded particles should move enough that we can track them in the flow. An additional beam irradiated a Cu backlighter foil with a 1-ns square pulse to illuminate the sample and track the motion as captured on the XRFC's positioned opposite the backlighter. During the 0.1-ns gate duration of the framing camera, we collected snapshots of the bead positions (Fig. 24) in combination with VISAR and SOP. We demonstrated in this LBS shot day that (1) the targets can be made with sufficient precision to have the beads placed in precise locations; (2) the beads can be resolved with the number of photons generated via area backlighting; and (3) pressures achieved with CH are suitable to generate flow. A driven bead shot was collected, but bead location and preliminary analysis are ongoing. It could be that the beads melted at the shock-compression conditions achieved. The time delay between framing strips was set to intervals over which we anticipated a modest but detectable displacement of the particles.

These results have been shared by a graduate student at poster sessions at the HED Summer School (August 2019) and at the Division of Plasma Physics Meeting (October 2019).

This work was performed under the auspices of the U.S. Department of Energy under Grant DE-SC0019329 within the joint HEDLP program.

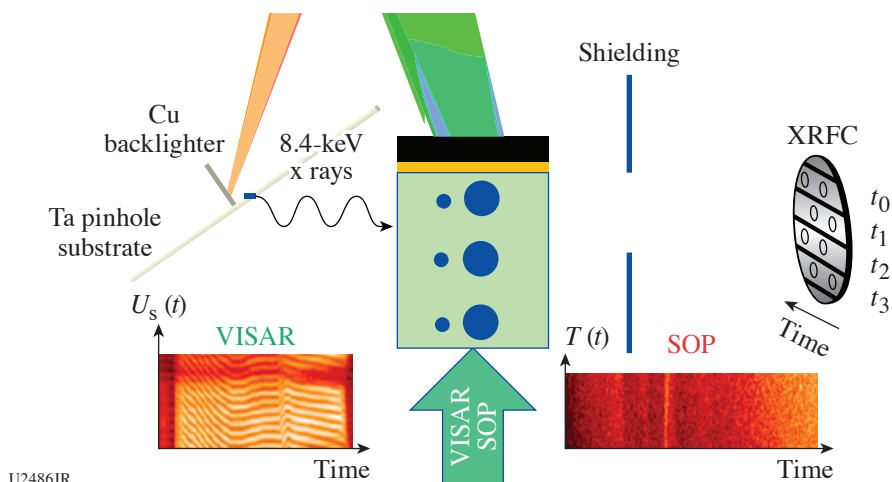


Figure 23
Schematic of a particle-tracking experiment conducted at LLE to date using an area backlighter and x-ray framing camera. The primary diagnostics are VISAR, XRFC, and SOP.

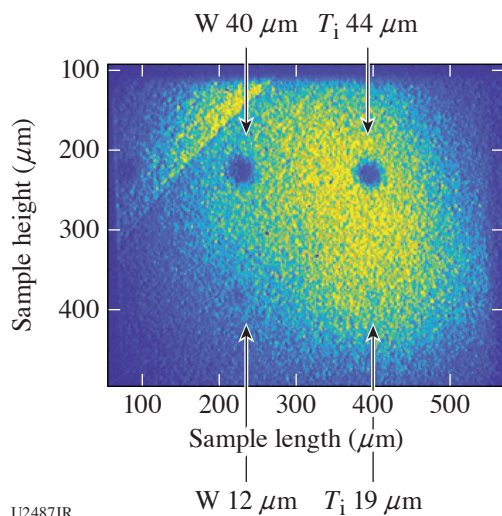


Figure 24
Image of high-Z beads placed along the side of the target.

X-Ray Phase-Contrast Imaging of Strong Shocks on OMEGA EP

Principal Investigator: W. Theobald (LLE)

Co-investigators: P. M. Nilson, A. Kar, R. Betti, and M. S. Wei, (LLE); L. Antonelli, M. Khan, and N. Woolsey (University of York, UK); R. Scott and K. Glize (RAL, UK); V. Bouffetier, L. Ceurvorst, A. Casner, O. Turianska, D. Batani, and F. Barbato (CELIA, University of Bordeaux, France); G. Rigon (Ecole Polytechnique, Palaiseau, France); and S. Atzeni (University of Rome “La Sapienza,” Italy)

X-ray phase contrast imaging (XPCI) is a technique that is widely used in biology and medicine. It is based on the phase shift induced by a density gradient in matter. When a density gradient is present perpendicularly to the propagation direction of the x ray, it deflects the x-ray beam in the opposite direction with respect to the density gradient. If we consider a density edge, the resulting XPCI image of this edge is located between a maximum and a minimum of the intensity profile. This effect is able to highlight every density interface and is not density dependent. Strong density gradients of very different densities can be probed at the same time. This makes this diagnostic more versatile compared to standard x-ray absorption radiography. Moreover, XPCI works with both monochromatic and broadband sources, which makes this technique an interesting tool for warm dense matter and HED physics studies. X-ray free-electron lasers and synchrotrons are the usual platform for XPCI experiments due to the

high-energy flux and the coherence of the beams. However, incoherent x-ray radiation sources can also be used for XPCI thanks to the lateral coherence, which is defined as

$$l_t \approx R \frac{\lambda}{s}, \quad (1)$$

where R is the source-object distance, λ is the photon wavelength, and s is the source size. It is clear from this formula that if one is able to use a small source size, not-too-hard x rays (several keV), and a setup that maximizes the source-object distance (which might be limited by the photon flux and other technical constraints), phase-contrast enhancement can be achieved. Moreover, if high-energy x rays are used, it is possible to shield the detector from target self-emission and focus the attention on the hydrodynamic evolution of the target. A successful proof-of-principle experiment was performed by some of the co-authors at the PHELIX laser at GSI, Germany, with a laser-driven bremsstrahlung source that provided experimental images of both the shock front and the rarefaction wave.³⁶ This was followed by an experiment (XPCI-EP-19A) that demonstrated x-ray phase contrast imaging on OMEGA EP, which is described here. The experiment developed the XPCI technique on OMEGA EP with short-pulse backlighters and used this technique to measure the density profile of a strong shock in a cylindrical CH target. Various backlighter targets containing Cu material were tested in order to optimize the x-ray phase contrast source. The experiment demonstrated a spatial resolution of $\sim 15 \mu\text{m}$ at sufficient photon energies (~ 8 to 9 keV) so that the images are not affected by the strong x-ray self-emission from the plasma corona. Figure 25 shows images of (a) a single and (b) a double laser-induced shock wave. Figure 25(c) shows the experimental setup. The two UV ($\lambda = 0.35\text{-}\mu\text{m}$) laser beams (B3, B4) provided an energy of 1250 J/beam in a 2-ns square pulse and were focused on the front side of a CH cylinder with a diameter of 1 mm and a length of 1 mm . The beams were equipped with SG8-0750 distributed phase plates that produced a laser spot with a diameter of $750 \mu\text{m}$ ($1/e$ value of peak fluence) and fluence distribution envelope that is well described by a super-Gaussian function with an order of 6.4 .

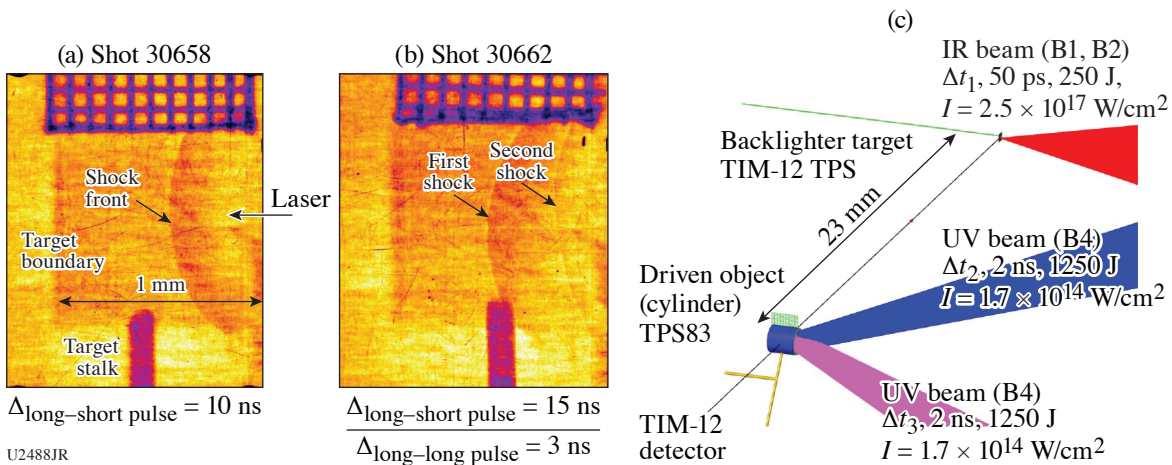


Figure 25

XPCI data of (a) a single and (b) a double laser-induced shock wave on OMEGA EP. (c) Setup of the XPCI experiment on OMEGA EP. The radiograph shown in (a) was taken 10 ns after the start of the UV beam, and the shock wave has propagated over several hundred microns in the CH target. The radiograph shown in (b) was taken at 15 ns after the start of the first UV pulse. The second UV pulse was launched at a 3-ns delay with respect to the first UV pulse.

The backlighter target consisted of a $5 \times 30 \times 300\text{-}\mu\text{m}^3$ small strip of Cu foil glued onto a $10\text{-}\mu\text{m}$ -thick CH substrate. Either IR beam B1 or B2 was focused normal onto the Cu strip with the strip aligned along the axis to TIM-14, which contained a passive imaging plate detector in a heavy metal shielded box (LLDI). The backlighter produced a strong emission between 8 and 9 keV predominately from the He_α and Ly_α resonance lines. The distance from backlighter to CH cylinder was 2.3 cm , and the distance from the CH cylinder to the IP detector was 1.4 m , providing a magnification of $60\times$.

Resolution Au grids mounted on the top of the cylinder provide a spatial fiducial and are used to infer the spatial resolution, which was found to be $15 \mu\text{m}$ in the horizontal direction and $18 \mu\text{m}$ in the vertical direction. The spatial resolution was limited

by the source size and how well the strip target could be aligned. The images show many scratches on the image plate (IP), which somehow degraded the image quality. The IP's were used multiple times before the experiment and the scratches accumulated from prior use. Future experiments will request fresh IP's in order to avoid these scratches.

The data were successfully reproduced by simulations of the UV beam interaction using the 2-D radiation hydrodynamic code *DUED*.³⁷ Figure 26(a) compares the experimental data (top) from the double-shock experiment and the simulated x-ray phase contrast image (bottom), showing good agreement of the general signal level and also the positions of both shock fronts. Figure 26(b) shows lineouts along the horizontal axis of the experimental data and the simulated data, showing the typical signal excursions that are caused by the phase enhancement. The hydrodynamic simulation results were post-processed with an XPCI code that is described in Ref. 36. The shock wave is not perfectly symmetric because both beams are not interacting with the target surface at normal incidence but with an angle of incidence of 23° with respect to the target normal from different directions. The data analysis is ongoing with planned comparison to other hydrodynamic codes, improvements of image filtering to enhance the image quality, and possible comparison with other XPCI codes. The XPCI-EP-19A experiment on OMEGA EP demonstrated x-ray phase-contrast imaging of strong shocks with sufficient contrast in a low-Z material.

This material is based upon work supported by the Department of Energy National Nuclear Security Administration under Award Number DE-NA0003856, the University of Rochester, and the New York State Energy Research and Development Authority.

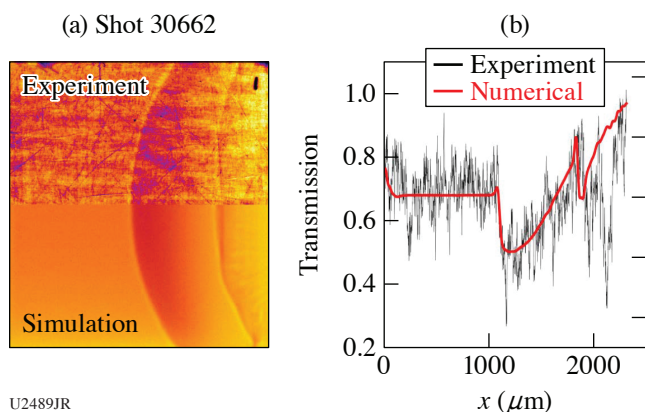


Figure 26

(a) Comparison of the experimental data (top) from the double-shock experiment and the simulated x-ray phase contrast image (bottom) shows good agreement of the general signal level and the positions of both shock fronts. (b) Lineouts along the horizontal axis of the experimental data and the simulated data show the typical signal excursions that are caused by the phase enhancement.

U2489JR

1. J. L. Shaw *et al.*, presented at the 61st Annual Meeting of the APS Division of Plasma Physics, Fort Lauderdale, FL, 21–25 October 2019.
2. G. J. Williams *et al.*, presented at the International Conference on High Energy Density Science (ICHED), Oxford, UK, 31 March–5 April 2019.
3. J. Kim *et al.*, “Dynamic Focusing of Laser Driven Positron Jets by Self-Generated Fields,” submitted to *New Journal of Physics*.
4. H. Chen *et al.*, *Phys. Rev. Lett.* **102**, 105001 (2009).
5. H. Chen *et al.*, *Phys. Rev. Lett.* **105**, 015003 (2010).
6. H. Chen *et al.*, *Phys. Plasmas* **21**, 040703 (2014).
7. O. V. Gotchev *et al.*, *Rev. Sci. Instrum.* **80**, 043504 (2009).
8. H. Chen *et al.*, *Phys. Rev. Lett.* **114**, 215001 (2015).
9. H. Chen *et al.*, *Phys. Plasmas* **22**, 056705 (2015).
10. H. Chen *et al.*, *High Energy Density Phys.* **7**, 225 (2011).
11. P. Tzeferacos *et al.*, *Nat. Commun.* **9**, 591 (2018).
12. *Report of the Workshop on High Energy Density Laboratory Physics Research Needs*, Office of Science and National Nuclear Security Administration, U.S. Department of Energy, Washington, DC (15–18 November 2009).

13. T. R. Boehly *et al.*, *Opt. Commun.* **133**, 495 (1997).
14. H. Witala and W. Glöckle, *Phys. Rev. C* **83**, 034004 (2011).
15. C. J. Forrest *et al.*, *Phys. Rev. C* **100**, 034001 (2019).
16. M. Vorabbi *et al.*, *Phys. Rev. C* **100**, 024304 (2019).
17. G. Fiksel *et al.*, *Phys. Rev. Lett.* **113**, 105003 (2014).
18. D. B. Schaeffer *et al.*, *Phys. Rev. Lett.* **119**, 025001 (2017).
19. S. A. Slutz *et al.*, *Phys. Plasmas* **17**, 056303 (2010).
20. D. D. Ryutov *et al.*, *Phys. Plasmas* **19**, 062706 (2012).
21. D. E. Fratanduono *et al.*, *Phys. Rev. B* **97**, 214105 (2018).
22. S. Root *et al.*, *Geophys. Res. Lett.* **45**, 3865 (2018).
23. R. F. Smith *et al.*, *Phys. Rev. Lett.* **101**, 065701 (2008).
24. J. S. Oakdale *et al.*, *Adv. Funct. Mater.* **27**, 1702425 (2017).
25. J. K. Wicks *et al.*, *Sci. Adv.* **4**, eaao5864 (2018).
26. D. Polsin, *LLE 2018 Annual Report, October 2019-September 2018*, 240, Laboratory for Laser Energetics, University of Rochester, Rochester, NY, LLE Document No. DOE/NA/1944-1450 (March 2019).
27. H. Tups and K. Syassen, *J. Phys. F: Met. Phys.* **14**, 2753 (1984).
28. S. Brygoo *et al.*, *J. Appl. Phys.* **118**, 195901 (2015).
29. H. Daido *et al.*, *Appl. Phys. Lett.* **51**, 2195 (1987).
30. G. Ren *et al.*, *Phys. Rev. Lett.* **118**, 165001 (2017).
31. M. Millot *et al.*, *Nat. Phys.* **14**, 297 (2018).
32. M. Millot *et al.*, *Nature* **569**, 251 (2019).
33. B. Militzer and H. F. Wilson, *Phys. Rev. Lett.* **105**, 195701 (2010).
34. V. A. Thomas and R. J. Kares, *Phys. Rev. Lett.* **109**, 075004 (2012).
35. D. S. Clark *et al.*, *Phys. Plasmas* **23**, 056302 (2016).
36. L. Antonelli *et al.*, *Europhys. Lett.* **125**, 35002 (2019).
37. S. Atzeni *et al.*, *Comput. Phys. Commun.* **169**, 153 (2005).